Journal of Sulfur Chemistry
Publication details, including instructions for authors and subscription information:
http://www.informaworld.com/smpp/title~content=t713926081

Synthesis, characterization and antibacterial activity of Pd(II), Pt(II) and Ag(I) complexes of 4-ethyl and 4-(*p*-tolyl)-1-(pyridin-2-yl)thiosemicarbazides

Ahmed A. El-Asmy[a]; Mohammad M. Hassanian[b]; Mohammad H. Abdel-Rhman[a]
[a] Chemistry Department, Faculty of Science, Mansoura University, Egypt [b] Chemistry Department, Industrial Education College, Beni-Suef University, Egypt

Online publication date: 07 April 2010

To cite this Article El-Asmy, Ahmed A. , Hassanian, Mohammad M. and Abdel-Rhman, Mohammad H.(2010) 'Synthesis, characterization and antibacterial activity of Pd(II), Pt(II) and Ag(I) complexes of 4-ethyl and 4-(*p*-tolyl)-1-(pyridin-2-yl)thiosemicarbazides', Journal of Sulfur Chemistry, 31: 2, 141 — 151
To link to this Article: DOI: 10.1080/17415990903569569
URL: http://dx.doi.org/10.1080/17415990903569569

Journal of Sulfur Chemistry
Vol. 31, No. 2, April 2010, 141–151

Taylor & Francis
Taylor & Francis Group

Synthesis, characterization and antibacterial activity of Pd(II), Pt(II) and Ag(I) complexes of 4-ethyl and 4-(*p*-tolyl)-1-(pyridin-2-yl)thiosemicarbazides

Ahmed A. El-Asmy[a]*, Mohammad M. Hassanian[b] and Mohammad H. Abdel-Rhman[a]

[a]*Chemistry Department, Faculty of Science, Mansoura University, Egypt;* [b]*Chemistry Department, Industrial Education College, Beni-Suef University, Egypt*

(*Received 12 October 2009; final version received 13 December 2009*)

Pd(II), Pt(II) and Ag(I) ions were found to form stable complexes with 4-(*p*-tolyl)- or 4-ethyl-1-(pyridin-2-yl)thiosemicarbazides (H*p*-TPTS or HEPTS). The complex structure was elucidated by analysis (elemental and thermal), spectroscopy (electronic, IR and ^{1}H NMR spectra) and physical measurements (magnetic susceptibility and molar conductance). The ligands coordinate to the metal ions as monobasic bidentate through nitrogen and sulfur atoms. The electronic spectra of the Pt(II) complexes in DMF showed a metal to ligand charge transfer transition at 11,935–13,260 cm^{-1}. The structural, electronic and vibrational features of HEPTS and H*p*−TPTS were discussed on the basis of semi-empirical quantum mechanic calculations [ZINDO/S and semi-empirical parameterization (PM3)]. The simulated IR and electronic spectra are found reasonable in accordance with the experimental data. Finally, the antibacterial activities of the ligands and their complexes were investigated and some were found promising.

Keywords: thiosemicarbazide; Pd(II) complexes; Pt(II) complexes; Ag(I) complexes; antibacterial activity

1. Introduction

Thiosemicarbazides constitute an important class of NS donors. The chemistry of these compounds was early explored (*1*) for their variable donor properties, structural diversity and biological applications. The coordination chemistry of a number of metal ions and a wide variety of complexes had been reported (*2–9*). Thiosemicarbazide complexes have anticancer and antimicrobial activity owing to their ability to diffuse through the semipermeable membrane of the cell lines. The enhanced effect may be due to the increase of lipophilicity of the complexes compared to the ligand (*5*, *10–12*). Thiosemicarbazides have been used for extraction and determination of some metal ions in biological and pharmacological samples (*13*, *14*). Following the discovery of the antitumor activity of *cis*-platin and related complexes, much interest has been focussed on the synthesis of more complexes. Pd(II) complexes, the analogs to *cis*-platin, are found efficient for clinical trials against tumors. However, *cis*-palladium complexes have high toxicity and lower

*Corresponding author. Email: aelasmy@yahoo.com

ISSN 1741-5993 print/ISSN 1741-6000 online

DOI: 10.1080/17415990903569569
http://www.informaworld.com

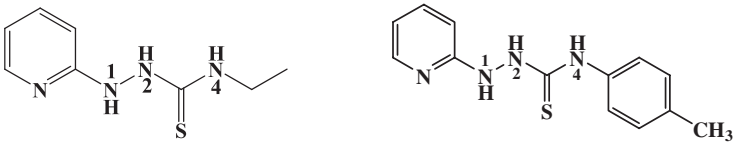

HEPTS H*p*-TPTS

Figure 1. 4-Ethyl and 4-(*p*-tolyl)-1-(pyridin-2-yl)thiosemicarbazide.

antitumor activity than Pt(II) complexes. Pd(II) chelates with NS donors were suggested as effective antitumor agents (*15*, *16*) due to their higher ability to bring the metal into DNA. In this respect, Pt(II) chelates are kinetically inert, while those of Ni(II), Zn(II), Cu(II), etc., do not have sufficient thermodynamic stability (*15*). 2-Hydrazinopyridine complexes were used in the delivery of cytotoxin for therapy or radionuclide for imaging (*17*, *18*). Rhenium complexes of 4-*t*-butyl- and 4-phenyl-1-(pyridin-2-yl)thiosemicarbazides were used for radiopharmaceutical applications. The crystal structure showed that the ligand containing phenyl derivative behaves as SN^1 donor where *t*-butyl behaves as SN^3N (*19*).

Cu(II) complexes of 4-ethyl-1-(pyridin-2-yl)thiosemicarbazide (HEPTS) were synthesized and characterized (*20*). This ligand was used for separation, preconcentration and determination of Cu(II) ions (*21*, *22*).

The present work aims to synthesize and characterize Pd(II), Pt(II) and Ag(I) complexes of 4-ethyl- and 4-(*p*-tolyl)-1-(pyridin-2-yl)thiosemicarbazide (HEPTS and H*p*-TPTS) and examining their antibacterial activities (Figure 1).

2. Results and discussion

The elemental analysis indicated the stoichiometry of the isolated complexes (Table 1). All have high melting points (>300 °C) and are insoluble in most common organic solvents but soluble in DMF and DMSO; Ag(I) complexes are partially soluble. The molar conductance values, in DMF, indicate non-electrolytes ($\Lambda_m = 5$–$10\ \Omega^{-1}\ cm^2\ mol^{-1}$).

Table 1. Elemental analysis of the ligands and their isolated complexes.

			Found %			Calcd. %		
Compound, formula (F. wt)	Color	M.p. (°C)	C	H	M	C	H	M
HEPTS, $C_8H_{12}N_4S$ (196.27)	Yellowish white	177	49.02	6.34	–	48.96	6.16	–
[Pd(EPTS)$_2$].4H$_2$O, $C_{16}H_{30}N_8O_4S_2Pd$ (569.01)	Green	>300	33.73	5.02	18.52	33.77	5.31	18.70
[Pt(EPTS)$_2$].5H$_2$O, $C_{16}H_{32}N_8O_5S_2Pt$ (675.68)	Reddish brown	>300	28.01	4.18	28.95	28.44	4.77	28.87
[Ag(EPTS)].EtOH, $C_{10}H_{17}N_4OSAg$ (349.20)	Brown	>300	34.42	5.29	30.44	34.40	4.91	30.89
H*p*-TPTS $C_{13}H_{14}N_4S$ (258.34)	White	167	59.82	5.11	–	60.44	5.46	
[Pd(*p*-TPTS)$_2$].4H$_2$O, $C_{26}H_{34}N_8O_4S_2Pd$ (693.15)	Green	>300	44.64	5.51	14.98	45.05	4.94	15.35
[Pt(*p*-TPTS)$_2$]·4H$_2$O, $C_{26}H_{34}N_8O_4S_2Pt$ (781.81)	Reddish brown	>300	39.62	4.12	24.52	39.94	4.38	24.95
[Ag(*p*-TPTS)]·EtOH, $C_{15}H_{19}N_4OSAg$ (411.27)	Brown	>300	43.37	4.86	25.98	43.81	4.66	26.23

2.1. *IR spectra*

The IR spectrum of H*p*-TPTS showed bands at 3267, 3170, 3135 and 725 cm^{-1} attributed to $\nu(N^4H)$, $\nu(N^1H)$, $\nu(N^2H)$ and ρ(NH), respectively (*4*, *23*). Also, the bands at 1595 (1522, 1449 and 782) cm^{-1} are assigned to $\nu(C{=}N)_{Py}$ (*24*) and thioamide (I, III and IV) (*4*), respectively, indicating that the ligands exist in the thione form. The $\nu(N^2H)$, and $\nu(C{=}N)_{Py}$ bands were found at lower wave numbers than those of HEPTS due to the involvement of these groups in intramolecular H-bonding (*25*). The most important spectral data of the ligands are listed in Table 2.

Careful comparison of the IR spectra of the ligands with their Pd(II), Pt(II) and Ag(I) complexes reveals the shift of $\nu(N^1H)$ to higher wavenumbers supporting its coordination (*26*). The new band at ~1635 cm^{-1}, assigned to $\nu(C{=}N^2)$, and the disappearance of $\nu(N^2H)$ and ν(C=S) indicate the thioenolization of the ligands (C−SH) and their coordination *via* sulfur atoms. The $\nu(C{=}N)_{py}$ appears more or less at the same position indicating its non-involvement in coordination. Thus, the ligands behave as a monobasic bidentate (NS donors) (*20*). A new band at 500–520 cm^{-1} is assigned to ν(M−N) (*26*, *27*). The nitrate bands in the Ag(I) complexes are absent (*28*). An angular structure is proposed for Ag(I) complexes.

2.2. ^{1}*H NMR spectra*

The ^{1}H NMR spectrum of H*p*-TPTS in DMSO-d_6 (Figure 2) showed the signals of the phenyl and pyridyl protons (Table 3) (*25*, *29*). The three singlet signals at 8.50, 9.61 and 9.76 ppm are attributed to the N^2H, N^1H and N^4H protons, respectively. It is observed that the N^2H signal appears in the aromatic region which confirms its involvement in intramolecular H-bond with the $N_{pyridyl}$. The other NH protons are shifted upfield due to the inductive effect of pyridyl and phenyl rings as electron donor groups (*25*). The $-CH_3$ protons appear as a singlet at 3.40 ppm.

The spectrum of [Pd(*p*-TPTS)$_2$].4H$_2$O in DMSO-d_6 (Figure 3) showed the disappearance of the N^2H signal and the downfield shift of N^1H indicating that the ligand exists in the thiol form with the involvement of N^1H in coordination. The pyridyl and phenyl protons appear more or less at the same position indicating that they are not involved in coordination to the metal ion (*30*).

Comparison of the spectrum of HEPTS in CD_3Cl (*20*) with its Pd(II) complex in DMSO reveals that the N^1H signal is shifted downfield while the N^2H disappeared confirming its thioenolization and involvement in coordination (*30*). The spectra indicate the presence of ethyl and pyridyl signals at the same position (Table 3).

Table 2. Infra-red spectral date of ligands and isolated solid complexes in KBr as well as calculated frequencies in the gaseous state.

	HEPTS					H*p*-TPTS				
Assignment	Exp.	PM3	Pd–EPTS	Pt–EPTS	Ag–EPTS	Exp.	PM3	Pd–*p*-TPTS	Pt–*p*-TPTS	Ag–*p*-TPTS
$\nu(OH)_{solv}$	–	–	3433	3432	3395	–		3439	3407	3377
$\nu(N^4H)$	3239	3350	3286	3282	3324	3267	3351	3343	3348	3240
$\nu(N^1H)$	3154	3255	3233	3260	3265	3170	3290	3215	3220	3200
$\nu(C{=}N^2)$	–		1637	1636	1635	–	–	1634	1636	1635
$\nu(C{=}N)_{Py}$	1604	1745	1607	1598	1595	1595	1746	1604	1598	1608
NHCS(I, III)	1519	1525	1531	1489	1461	1522	1510	1515	1515	1500
	1446	1496	1437	1448	1436	1449	1431	1440	1444	1440
ν(C=S)	798	842	–	–	–	782	798	–	–	–
ρ(NH)	773	772	752	750	776	725	763	750	748	760
	736									

Note: H*p*-TPTS: N^2H 3135 cm^{-1}.

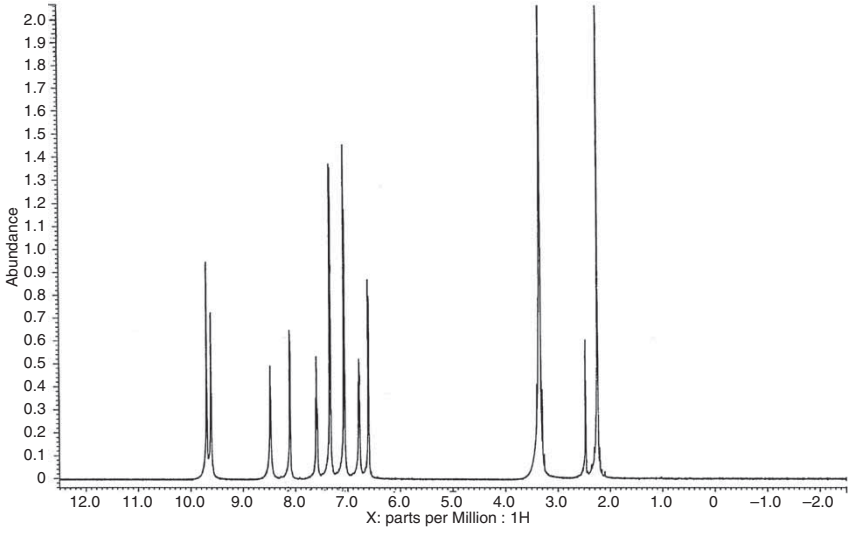

Figure 2. ^{1}H NMR spectrum of H*p*-TPTS in DMSO-d_6.

Table 3. ^{1}H NMR spectral data of HEPTS and H*p*-TPTS and their Pd(II) complexes (ppm).

Compound	N^1H	N^2H	N^4H	$H^3{}_{Py}$	$H^4{}_{Py}$	$H^5{}_{Py}$	$H^6{}_{Py}$	$-CH_2-$	$-CH_3$
HEPTS	6.87	7.62	–	6.87	7.62	6.87	8.09	3.63	1.75
$[Pd(EPTS)_2]\cdot 4H_2O$	8.49	–	7.76	6.71	7.17	7.56	8.17	3.46	1.46
Compound	N^1H	N^2H	N^4H	$H^3{}_{Py}$	$H^4{}_{Py}$	$H^5{}_{Py}$	$H^6{}_{Py}$	$H^2{}_{Bz}$	$H^3{}_{Bz}$
H*p*-TPTS	9.61	8.50	9.76	6.60	7.60	7.04	8.10	7.32	7.59
$[Pd(p\text{-}TPTS)_2]\cdot 4H_2O$	10.14	–	9.77	6.79	7.81	7.15	8.32	7.33	7.60

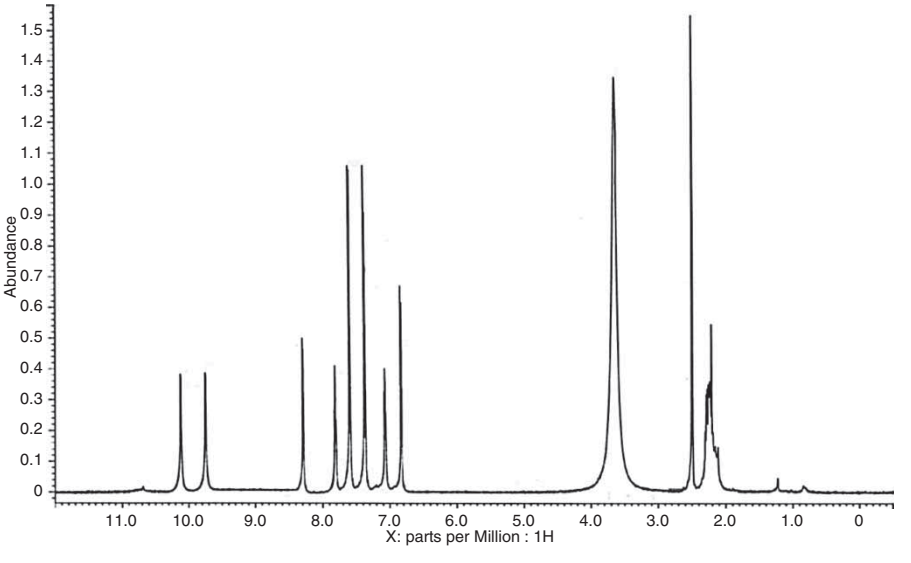

Figure 3. ^{1}H NMR spectrum of $[Pd(p\text{-}TPTS)_2]$. $4H_2O$ in DMSO-d_6.

2.3. *Electronic spectra*

The electronic spectra of HEPTS and H*p*-TPTS, in DMF, showed bands at 35,460–36,765, 31,950–32,260, 30,305–31,950 and 23,200–24,940 cm^{-1} attributed to $(\pi \rightarrow \pi^*)_{Py}$, $(\pi \rightarrow \pi^*)_{CS}$ (*24*, *25*), $(n \rightarrow \pi^*)_{Py}$ and $(n \rightarrow \pi^*)_{CS}$ (*24*, *31*), respectively. Moreover, the spectrum of H*p*-TPTS in DMF showed another band at 33,780 cm^{-1} assigned to $(\pi \rightarrow \pi^*)_{Ph}$ (Table 4). The appearance of two bands at 32,575–33,670 and 28,655–29,411 cm^{-1} attributed to $(\pi \rightarrow \pi^*)$ and $(n \rightarrow \pi^*)$ of the newly formed ($C{=}N^2$) supports the thiol form of the ligand (*24*, *31*).

In the spectra of square planar Pd(II) and Pt(II) complexes, three spin-allowed singlet–singlet d–d transitions were predicted. The ground state is $^1A_{1g}$ and the excited states corresponding to the three transitions are $^1A_{2g}$, $^1B_{1g}$ and ^1E_g. Strong charge transfer transitions interfere and prevent the observation of all the expected bands (*32*). The spectra of Pd(II) complexes in DMF showed two bands at 24,875–25,250 and 18,450–18,520 cm^{-1} attributed to ligand-metal charge transfer (LMCT) (overlapped with $^1A_{1g} \rightarrow {}^1E_g$) and $^1A_{1g} \rightarrow {}^1A_{2g}$ (*32*, *33*). In Nujol, the spectra showed the three bands assignable to LMCT with d–d transitions (Table 4). The spectra of Pt(II) complexes in DMF showed two bands at 24,040–24,450 and 11,930–13,260 cm^{-1} attributed to LMCT (overlapped with $^1A_{1g} \rightarrow {}^1E_g$) and MLCT (*30*), respectively. In Nujol, the spectra showed

Table 4. The electronic spectral bands of ligands and its complexes observed in DMF, Nujol and the gas state (ZINDO/S calculations).

Compound	Solvent	Bands [ZINDO/S estimated] (assignment)	ν_2/ν_1
HEPTS	DMF	35,460 [35,971] $(\pi-\pi^*)_{Py}$; 31,950 [31,949] $(\pi-\pi^*)_{CS}$; 30,865 [27,027] $(n-\pi^*)_{Py}$; 24,940 [25,010] $(n-\pi^*)_{CS}$	–
$[Pd(EPTS)_2]\cdot 4H_2O$	DMF	36,765 $(\pi-\pi^*)_{Py}$; 32,575 $(\pi-\pi^*)^2_{CN}$; 30,770 $(n-\pi^*)_{Py}$; 24,875 ($^1A_{1g} \rightarrow {}^1E_g$ + LMCT); 18,450 ($^1A_{1g} \rightarrow {}^1A_{2g}$ + LMCT)	1.28
	Nujol	25,640 ($^1A_{1g} \rightarrow {}^1E_g$ + LMCT); 23,475 ($^1A_{1g} \rightarrow {}^1B_{1g}$ + LMCT); 18,315 ($^1A_{1g} \rightarrow {}^1A_{2g}$ + LMCT)	
$[Pt(EPTS)_2]\cdot 5H_2O$	DMF	36,765 $(\pi-\pi^*)_{Py}$; 33,115 $(\pi-\pi^*)^2_{CN}$; 30,305 $(n-\pi^*)_{Py}$; 24,450 ($^1A_{1g} \rightarrow {}^1E_g$ + LMCT); 17,185 ($^1A_{1g} \rightarrow {}^1A_{2g}$ + LMCT); 13,260 (MLCT)	1.13
	Nujol	24,270 ($^1A_{1g} \rightarrow {}^1E_g$ + LMCT); 21,645 ($^1A_{1g} \rightarrow {}^1B_{1g}$ + LMCT); 19,230 ($^1A_{1g} \rightarrow {}^1A_{2g}$ + LMCT)	
[Ag(EPTS)]·EtOH	DMF	36,500 $(\pi-\pi^*)_{Py}$; 33,670 $(\pi-\pi^*)^2_{CN}$; 30,395 $(n-\pi^*)_{Py}$; 29,760 $(n-\pi^*)^2_{CN}$; 26,110 (LMCT)	–
	Nujol	24,875 (LMCT); 21,100 (LMCT)	
H*p*-TPTS	DMF	36,500 [35,335] $(\pi-\pi^*)_{Py}$; 33,785 [33,557] $(\pi-\pi^*)_{Ph}$; 32,260 [31,546] $(\pi-\pi^*)_{CS}$; 30,490 [28,818] $(n-\pi^*)_{Py}$; 23,200 [23,474] $(n-\pi^*)_{CS}$	–
$[Pd(p\text{-}TPTS)_2]\cdot 4H_2O$	DMF	35,970 $(\pi-\pi^*)_{Py}$; 33,900 $(\pi-\pi^*)_{Ph}$; 31,150 $(n-\pi^*)_{Py}$; 29,585 $(n-\pi^*)^2_{CN}$; 25,250 ($^1A_{1g} \rightarrow {}^1E_g$ + LMCT); 18,520 ($^1A_{1g} \rightarrow {}^1A_{2g}$ + LMCT)	1.15
	Nujol	23,925 ($^1A_{1g} \rightarrow {}^1E_g$ + LMCT); 21,645 ($^1A_{1g} \rightarrow {}^1B_{1g}$ + LMCT); 18,870 ($^1A_{1g} \rightarrow {}^1A_{2g}$ + LMCT)	
$[Pt(p\text{-}TPTS)_2]\cdot 4H_2O$	DMF	36,230 $(\pi-\pi^*)_{Py}$; 33,900 $(\pi-\pi^*)_{Ph}$; 31,950 $(n-\pi^*)_{Py}$; 29,675 $(n-\pi^*)^2_{CN}$; 24,040 ($^1A_{1g} \rightarrow {}^1E_g$ + LMCT); 11,935 (MLCT)	1.26
	Nujol	25,000 ($^1A_{1g} \rightarrow {}^1E_g$ + LMCT); 21,550 ($^1A_{1g} \rightarrow {}^1B_{1g}$ + LMCT); 17,065 ($^1A_{1g} \rightarrow {}^1A_{2g}$ + LMCT)	
[Ag(*p*-TPTS)]·EtOH	DMF	36,500 $(\pi-\pi^*)_{Py}$; 34,245 $(\pi-\pi^*)_{Ph}$; 31,545 $(n-\pi^*)_{Py}$; 28,655 $(n-\pi^*)^2_{CN}$; 26,385 (LMCT)	–
	Nujol	26,595 (LMCT); 23,585 (LMCT)	

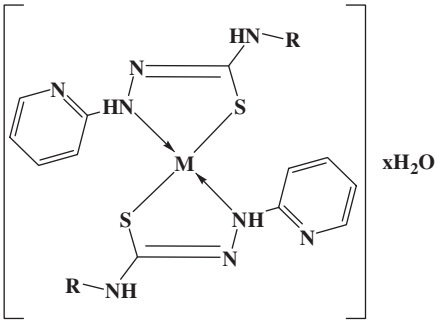

M = Pd(II), R = Et and *p*-tolyl, x = 4
M = Pt(II), R = Et, x = 5
M = Pt(II), R = *p*-tolyl, x = 4

Figure 4. Proposed structure of Pd(II) and Pt(II) complexes.

the bands at 25,000–24,270, 21,645–21,550 and 19,230–17,065 cm^{-1} assignable to the LMCT (overlapped with $^1A_{1g} \rightarrow {}^1E_g$, $^1A_{1g} \rightarrow {}^1B_{1g}$ and $^1A_{1g} \rightarrow {}^1A_{2g}$) transitions, respectively. The ν_2/ν_1 values lie in the 1.13–1.28 range, comparable with the values reported for the square-planar Pd(II) and Pt(II) complexes (*33*) (Figure 4).

The spectra of Ag(I) complexes in DMF showed a charge transfer band at 26,110–26,385 cm^{-1} (*32*).

2.4. *Thermal analysis*

The thermogravimetry (TG) curve of H*p*-TPTS indicates a thermal stability till 170 °C (its melting point is 178 °C). The curve showed three decomposition steps at 191 °C, 257 °C and 501 °C corresponding to the loss of PyNHNHC (Found 44.94; Calcd. 46.89%), PhNHS+3H (Found 50.75, Calcd. 49.60%) and complete decomposition of the ligand.

The TG thermograms of the isolated complexes were taken as a proof for the water molecules to be outside the coordination sphere which was lost at 70–248 °C with mid-point at ~110 °C (Table 5). Generally, the complexes showed a higher thermal stability than the ligands where the beginning of decomposition was observed at 190–266 °C. Complete data of all decomposition steps are shown in Table 5.

2.5. *Kinetic and thermodynamic data*

To evaluate the kinetic and thermodynamic parameters for the different thermal decomposition steps, the Coats–Redfern (*34*) and Horowitz–Metzger (*35*) equations are employed. The data of activation enthalpy (ΔH^*), the activation entropy (ΔS^*) and the free energy of activation (ΔG^*) are determined and presented in Table 5. From the results, one can point out the following remarks:

The ΔE^* values reveal high stability of the chelates due to their covalent bond character.
The positive sign of ΔH^* indicates that the decomposition stages are endothermic processes.
The positive sign of ΔG^* reveals that all the decomposition steps are non-spontaneous processes.
The negative values of ΔS^* suggest the residue after decomposition is more ordered than the starting ones.

Table 5. Thermal analysis data and thermodynamic parameters of ligands and complexes.

	Thermal analysis			Kinetic parameters						
Compound	Temp.	Wt%	Assignment	ΔE^*	ΔS^*	ΔH^*	ΔG^*	A	R	SD
H*p*-TPTS	168–214	44.94	PyNHNHC (46.89)	–	–	–	–	–	–	–
	214–300	50.75	3H + PhNHS (49.60)	143.94 (152.78)	61.20	139.52	106.98	1.74E16	0.9835 (0.9818)	0.2918 (0.3243)
	300–702	4.31	C (4.65)	–	–	–	–	–	–	–
[Pd(*p*-TPTS)$_2$]·4H$_2$O	28–200	9.99	4H$_2$O (10.40)	22.72 (28.24)	−94.93	19.49	56.33	8.89E7	0.9822 (0.9817)	0.1266 (0.1587)
	200–500	30.09	2(NHPhCH$_3$) (30.63)	46.64 (52.66)	−217.64	41.46	177.09	55.57	0.9863 (0.9819)	0.2092 (0.2458)
	500–750	23.21	2Py (22.53)	44.93 (65.77)	−196.01	37.50	212.54	1073.49	0.9854 (0.9900)	0.0655 (0.0778)
	Res.	36.71	Pd(CHN$_2$S)$_2$ (36.44)	–	–	–	–	–	–	–
[Pt(*p*-TPTS)$_2$]·4H$_2$O	28–190	10.10	4H$_2$O (9.22)	33.47 (28.24)	−235.83	30.37	118.45	3.74	0.9822 (0.9817)	0.2498 (0.1587)
	190–490	27.89	2(NHPhCH$_3$) (27.16)	46.64 (51.47)	−217.64	41.46	177.09	55.57	0.9863 (0.9864)	0.2092 (0.1769)
	490–740	19.08	2Py (19.98)	–	–	–	–	–	–	–
	Res.	42.94	Pt(CHN$_2$S)$_2$ (43.64)	–	–	–	–	–	–	–
[Pd(EPTS)$_2$]·4H$_2$O	28–248	12.81	4H$_2$O (12.67)	24.47 (23.16)	−214.26	21.33	102.32	50.64	0.9787 (0.9875)	0.2562 (0.1979)
	266–344	16.12	2(NHEt) (15.49)	124.53 (130.91)	−132.80	119.67	197.29	1.41E6	0.9844 (0.9837)	0.1224 (0.1345)
	344–744	26.11	2Py (27.45)	–	–	–	–	–	–	–
	Res.	44.80	Pd(CHN$_2$S)$_2$ (44.37)	–	–	–	–	–	–	–
[Pt(EPTS)$_2$]·5H$_2$O	28–230	12.58	5H$_2$O (13.12)	37.06 (33.57)	−236.90	33.79	126.96	3.46	0.9819 (0.9861)	0.2615 (0.1658)
	240–450	12.84	2(NHEt) (13.05)	40.61 (50.29)	−213.29	35.51	166.36	92.35	0.9866 (0.9843)	0.1182 (0.1583)
	450–750	31.66	2(Py + CN) (30.19)	–	–	–	–	–	–	–
	Res.	42.92	Pt(NS)$_2$ (42.48)	–	–	–	–	–	–	–

Note: Values between brackets were calculated by Horowitz–Metzger equation.

2.6. *Molecular modeling and spectral analysis data*

The geometric optimization structure of HEPTS was discussed in the previous work (*22*). The H*p*-TPTS modeling indicates a non-planar structure (Figure 5). On comparison with HEPTS, it is observed that the pyridyl nitrogen atom is involved in intramolecular H-bond [HN^2 . . .. H(24)]; the phenyl ring is perpendicular to the pyridyl ring and S(11) is in the same direction with the pyridyl nitrogen.

Also, the molecular modeling of [Pd(*p*-TPTS)$_2$].4H_2O and [Pd(EPTS)$_2$]·4H_2O is drawn in Figures 1S and 2S (supplementary material, online only). The data of their bond lengths (Table 1S) revealed that: (i) the bond lengths of N^4-H, N^1-H, $C_{Et}-N^4$ and $(C=N)_{Py}$ of the two Pd(II) complexes are quite close to those of the corresponding ligand which clearly indicates that they are not affected by the complex formation. (ii) The $C_{Py}-N^1$ bond lengths are found long which attributed to its involvement in coordination. (iii) The Pd−S and Pd−N bond lengths are similar to those reported earlier from X-ray crystallography (*9*).

The electrostatic potential calculations of the ligands showed that N and S atoms have negative potentials that support their involvement in coordination (Figure 6). The Mulliken charge density distributions in the ligands and their complexes are listed in Table 2S. The selected angles and the molecular parameters are displayed in Tables 3S–6S.

2.7. *Antibacterial activity*

The ligands and their complexes were tested to show their antibacterial and antifungal activities; the obtained values (mm) were compared with gentamicin. The experiments showed no antifungal activity towards *Asperigallus ochraceus*, *Staphylococcus aureus* and *Bacillus subtilis* as Gram positive and *Escherichia coli* and *Pseudomonas aeruginosa* as Gram negative are the tested bacteria. HEPTS has activity against *S. aureus*, whereas H*p*-TPTS has no activity. The Pd(II) and Pt(II) complexes of H*p*-TPTS showed higher activity than HEPTS complexes and

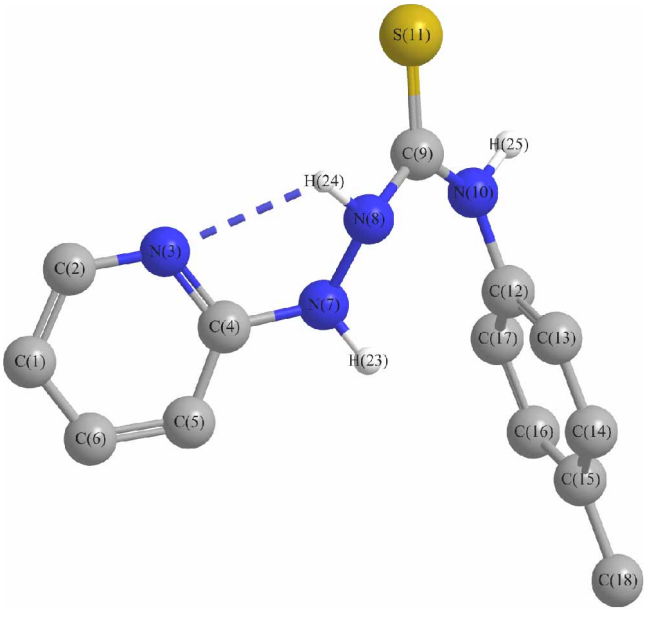

Figure 5. The PM3-optimized structure of H*p*-TPTS.

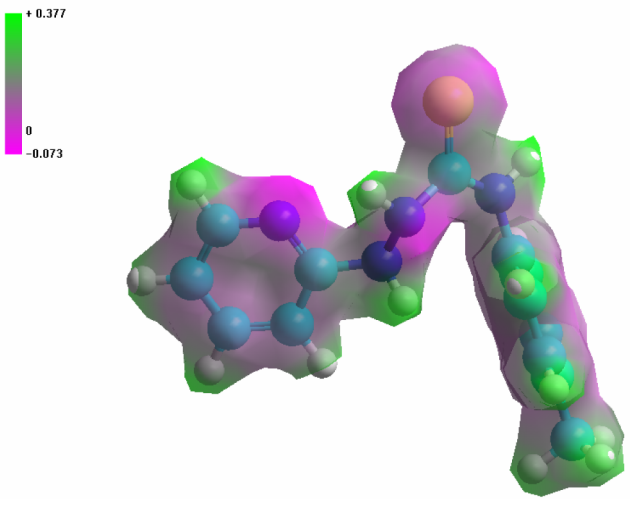

Figure 6. Electrostatic potential diagram of PM3-optimized H*p*-TPTS (colour online).

Table 6. Antibacterial activity of ligands and its complexes.

	Gram -ve		Gram +ve	
Complexes	*S. aureus*	*B. subtilis*	*E. coli*	*P. aeruginosa*
Gentamicin	25.9	19.8	20.0	23.6
HEPTS	15.8	19.4	–	–
$[Pd(EPTS)_2]\cdot 4H_2O$	16.3	20.1	12.0	–
$[Pt(EPTS)_2]\cdot 5H_2O$	16.0	20.5	12.4	–
[Ag(EPTS)]·EtOH	15.2	18.8	13.9	11.8
H*p*-TPTS	–	13.7	12.5	11.4
$[Pd(p\text{-}TPTS)_2]\cdot 4H_2O$	17.5	27.1	26.0	30.4
$[Pt(p\text{-}TPTS)_2]\cdot 4H_2O$	18.8	28.5	25.7	29.5
[Ag(*p*-TPTS)]·EtOH	–	14.9	16.8	14.8

gentamicin against all bacteria except *S. aureus*. The complexes have activity more than the ligands against *B.subtilis* bacteria, and the H*p*-TPTS complexes have nearly double activity (Table 6). On the other hand, HEPTS and its complexes showed no activity against *P. aeruginosa* except [Ag(EPTS)]EtOH while the complexes of H*p*-TPTS showed more activity. Generally, the data reveal the higher activity of H*p*-TPTS complexes than HEPTS complexes (Table 6). Comparing the data with previous data (*20*) indicates that Pd(II), Pt(II) and Ag(I) complexes derived from HEPTS showed more activity against Gram-negative bacteria than the ligand and its Cu(II) complexes.

3. Conclusion

4-Ethyl- or 4-*p*-tolyl-1-(pyridin-2-yl)thiosemicarbazides have been introduced as chelating agents for the formation of Ag(I), Pd(II) and Pt(II) complexes. The complexes have the formulae: $[Pd(EPTS)_2]\cdot 4H_2O$, $[Pd(p\text{-}TPTS)_2]\cdot 4H_2O$, $[Pt(EPTS)_2]\cdot 5H_2O$, $[Pt(p\text{-}TPTS)_2]\cdot 4H_2O$, [Ag(EPTS)]·EtOH and [Ag(*p*-TPTS)]·EtOH. The Pd(II) and Pt(II) complexes have a square-planar geometry while Ag(I) complexes have angular geometry. All compounds were found

promising for antibacterial activity especially [Pd(p-TPTS)$_2$].4H$_2$O and [Pt(p-TPTS)$_2$].4H$_2$O. The *in vitro* activity of Pd(II) complexes of steroidal thiosemicarbazone have values against *E. coli* less than our values.

4. Experimental

4.1. *Apparatus and reagents*

The IR spectra were recorded on a Mattson 5000 FT–IR spectrophotometer. The electronic spectra were measured on a Unicam UV–VIS spectrophotometer UV$_2$. The ^{1}H NMR spectra of HEPTS (in CDCl$_3$); HpTPTS and its Pd(II) complexes, in DMSO-d_6, were recorded on EM-390 (200 MHz) and Jeol Delta2 (500 MHz) spectrometers, respectively. Thermogravimetric analysis was performed using an automatic recording thermo balance, type 951 DuPont; samples were subjected to heat on a rate of 10 °C min^{-1} (25–750 °C) in N$_2$. Carbon and hydrogen content of the ligands and their complexes was determined at the Microanalytical Unit, Mansoura University, Egypt. Pd(II), Pt(II) and Ag(I) contents were determined using the Perkin Elmer 2380 flame atomic absorption spectrometer (Vernon Hills) with a conventional 10 cm slit burner head for air acetylene flame and Pye Unicam (England) hollow cathode lamps for the investigated elements were used as spectral radiation sources (where $\lambda = 244.8$, 266 and 328.1 nm and current = 15, 15 and 4 mA for Pd(II), Pt(II) and Ag(I), respectively). All salts and reagents used were purchased from Fluka, Aldrich or Merck.

4.2. *Synthesis of the ligands*

HEPTS was prepared as previously reported (*20*). Hp-TPTS was prepared by heating under reflux of a mixture of 2-hydrazinopyridine (0.1 mol) and p-tolylisothiocyanate (0.1 mol) in absolute ethanol for 2 h. On cooling, the yellowish white crystals were formed, filtered off, washed with ethanol and diethyl ether and recrystallized from ethanol (m.p. 167 °C; yield 95%). The purity of the compound (Figure 1) was checked by thin layer chromatography.

4.3. *Synthesis of complexes*

On mixing HEPTS or Hp-TPTS (0.01 mol) in ethanol (20 mL) with 0.01 mol of K_2PdCl_4, K_2PtCl_4 or $AgNO_3$, in water (5 mL), dark green, red break or brown precipitates were immediately formed. The reaction mixture was heated under reflux for 1 h on a water bath. The precipitates were filtered off after cooling, washed successfully with ethanol then diethyl ether, dried and preserved in a vacuum desiccator over anhydrous calcium chloride.

4.4. *Computational details*

All theoretical calculations of the quantum chemistry were performed using HyperChem 7.51 program system. First, molecular geometries of the ligand and its Pd(II) complexes were optimized by PM3 using the Polak-Ribiere algorithm in restricted RHF-SCF, set to terminate at a root mean square (RMS) gradient of 0.01 kcal Å^{-1} mol^{-1} and convergence limit was fixed to 1×10^{-8} kcal mol^{-1}. Secondly, the vibrational analysis and electronic spectra of ligands were performed by PM3 and RHF-SCF ZINDO/S calculations, respectively. The configuration interaction was limited to 10 occupied and 10 unoccupied orbitals.

4.5. *Antibacterial activity*

The ligands and their complexes have been tested as antibacterial agents at the Department of Microbiology, Faculty of Pharmacy, Mansoura University. The seeded agar plates were prepared by putting 50 mL portion of inoculated agar into 15 cm Petri dishes and allowed to solidify. Cups were made to receive 25 μL of the reagent solution and allowed to diffuse and incubated at 37 °C for 24 h. The inhibition zone was measured (*36*) and compared with that of gentamicin solution (commercial antibiotic, Memphis Co., Egypt, 1000 μg mL^{-1}). The experimental control was DMF.

References

(1) Gingras, B.A.; Somorjai, R.L.; Bayley, C.H. *Can. J. Chem.* **1961,** *39,* 973–985.
(2) Al-Gammal, O.A.; El-Asmy, A.A. *J. Coord. Chem.* **2008,** *61,* 2296–2306.
(3) Campbell, M.J.M. *Coord. Chem. Rev.* **1975,** *15,* 279–319.
(4) El-Metwally, N.M.; El-Shazly, R.M.; Gabr, E.; El-Asmy, A.A. *Spectrochim. Acta: A* **2005,** *61,* 1113–1119.
(5) West, D.X.; Padhye, S.; Sonawane, P.B. *Struct. Bond. (Berlin, Ger.)* **1991,** *76,* 4–50.
(6) Abou-Hussen, A.A.; Saad, I.M.; El-Metwally, N.M.; El-Asmy, A.A. *J. Coord. Chem.* **2005,** *58,* 1735–1749.
(7) Casas, J.S.; Garcia-Tasende, M.S.; Sordo, J. *J. Coord. Chem. Rev.* **2000,** *209,* 197–261.
(8) El-Metwally, N.M.; Al-Hazmi, G.A.; El-Asmy, A.A. *Transition Met. Chem.* **2006,** *31,* 673–680.
(9) Lobana, T.S.; Sharma, R.; Bawa, G.; Khanna, S. *Coord. Chem. Rev.* **2009,** *253,* 977–1055.
(10) Beraldo, H.; Gambino, D. *Min. Rev. Med. Chem.* **2004,** *4,* 31–39.
(11) Ferrari, M.B.; Bisceglie, F.; Fava, G.G.; Pelosi, G.; Tarasconi, P.; Albertini, R.; Pinelli, S. *J. Inorg. Biochem.* **2002,** *89,* 36–44.
(12) Seleem, H.S.; El-Shetary, B.A.; Khalil, S.M.E.; Mostafa, M.; Shebl, M. *J. Coord. Chem.* **2005,** *58,* 479–493.
(13) Akl, M.A.; Ismael, D.S.; El-Asmy, A.A. *Microchem. J.* **2006,** *83,* 61–69.
(14) Saad, E.M.; El-Shahwai, M.S.; Saleh, H.; El-Asmy, A.A. *Transition Met. Chem.* **2007,** *32,* 155–162.
(15) Blower, P.J.; Dilworth, J.R.; Maurer, R.I.; Mullen, G.D.; Reynolds, C.A.; Zheng, Y. *J. Inorg. Biochem.* **2001,** *85,* 15–22.
(16) Garoufis, A.; Hadjikakou, S.K.; Hadjiliadis, N. *Coord. Chem. Rev.* **2009,** *253,* 1384–1397.
(17) Das, M.; Livingstone, S.E. *Br. J. Cancer* **1978,** *37,* 466–470.
(18) Banerjee, S.R.; Maresca, K.P.; Francesconi, L.; Valliant, J.; Bbich, J.W.; Zubieta, J. *J. Nucl. Med. Biol.* **2005,** *32,* 1–20.
(19) Clarke, C.; Cowley, A.R.; Dilworth, J.R.; Donnelly, P.S. *J. Chem. Soc. Dalton Trans.* **2004,** 2402–2403.
(20) Hassanian, M.M.; Abdel-Rhman, M.H.; Gabr, I.M.; El-Asmy, A.A. *Spectrochim. Acta: A* **2008,** *71,* 73–79.
(21) Hassanian, M.M.; Abdel-Rhman, M.H.; Gabr, I.M.; El-Asmy, A.A. *Transition Met. Chem.* **2007,** *32,* 1025–1029.
(22) Hassanian, M.M.; Abdel-Rhman, M.H.; Gabr, I.M.; El-Asmy, A.A. *J. Chem. Eng. Data* **2009,** *54,* 1277–1283.
(23) Nakamoto, K. *Infrared and Raman Spectra of Inorganic and Coordination Compounds*, 5th ed.; John Wiley and Sons: New York, 1997; Part III.
(24) Silverston, R.M.; Bassler, C.G.; Morrill, T.C. *Spectrometric Identification of Organic Compound*; John Wiley: New York, 1974; Chapters 3 and 4.
(25) Valdés-Martínez, J.; Hernàndez-Ortega, S.; West, D.X.; Ackerman, L.J.; Swearingen, J.K.; Hermetet, A.K. *J. Mol. Struct.* **1999,** *478,* 219–226.
(26) Mortel, E. *Coordination Chemistry*; Van Nostrand Reinhold: New York, 1971; Vol. 1, Chapter 3.
(27) Mendes, I.C.; Teixeira, L.R.; Lima, R.; Carneiro, T.G.; Beraldo, H. *Transition Met. Chem.* **1999,** *24,* 655–658.
(28) Ramos, J.M.; Viana, R.M.; Tellez, C.A.; Pereira, W.C.; Izolani, A.O.; da Silva, M.I.P. *Spectrochim. Acta: A* **2006,** *65,* 433–438.
(29) Perera, S.D.; Fernandez-Sanchez, J.J., Shaw, B.L. *Inorg. Chim. Acta* **2001,** *325,* 175–178.
(30) Bhowmik, S.R.; Gangopadhyay, S.; Gangopadhyay, P.K. *J. Coord. Chem.* **2005,** *58,* 795–801.
(31) Seena, E.B.; Kurup, M.R.P. *Polyhederon* **2007,** *26,* 829–836.
(32) Lever, A.B.P. *Inorganic Electronic Spectroscopy*, 2nd ed.; Elsevier: Amsterdam, 1984; Chapter 9.
(33) Offiong, O.E.; Martelli, S. *Transition Met. Chem.* **1997,** *22,* 263–269.
(34) Coats, A.W.; Redfern, J.P. *Nature* **1964,** *201,* 68–69.
(35) Horowitz, H.H.; Metzger, G. *Anal. Chem.* **1963,** *35,* 1464–1468.
(36) Collee, J.G.; Fraser, A.G.; Marmion, B.P.; Simmons, A. *Mackie and McCartney; Practical Medical Microbiology*, 14th ed.; Churchill: New York, 1996; Chapter 7.